MEASUREMENT OF ROTOR MODES USING SMART STRUCTURES TECHNOLOGY.

C Hatch and T J Griffiths.

Defence Evaluation and Research Agency.
Farnborough, England.

Abstract

The development of state of the art rotor performance analysis tools requires extensive validation of the techniques used as part of the formal acceptance procedure. There are very few data of good quality available for this purpose and special consideration given to the new methods sometimes requires the generation of experimental data not previously measured. One of the new approaches employing rotor modes forms such a special consideration (Ref 1).

This work addresses the shortfall in measured rotor mode data and using smart structures technology develops a modal testing technique applicable to rotating systems. Measurement of the modes of a rotor whilst spinning has generally been confined to single blade measurements, however, the technique using piezo-ceramic actuators to excite all the rotor blades simultaneously whilst measuring rotor blade strain gauge responses provides a complete rotor modal analysis.

Rotor mode shapes, frequency and damping values are presented for the second and third flapwise bending modes at a selection of rotor speeds through to 600 rpm. Comparisons are made with conventional modal testing methods for a stationary rotor and the PZT actuators are shown to have some advantages over conventional electromagnetic shakers. More tests using a different PZT attachment are required to measure the system torsion modes and further developments are suggested to improve both the technique and data quality.

Introduction

The design of new, high performance rotor systems on modern helicopters demands the most up-to-date analysis tools. The Coupled Rotor Fuselage Model (CRFM) analysis suite of programs (Ref 1) developed jointly by the DRA and GKN Westland Helicopters incorporates the latest theoretical developments to enable a comprehensive rotor analysis to be performed. The CRFM approach uses complete rotor models to improve the predictive capability, rather than the single blade analyses of the past.

Confidence in these new tools can only be gained by validation of the theoretical methods over a wide range of configurations. This report describes an experiment performed using smart structures technology to obtain modal data of a rotor system for comparison with the CRFM. The rotor system used, based on a 2.2 m diameter model scale hub with 4 blades, is shown in figure 4 and described in (Ref 2).

The difficulties in measuring mode frequencies and shapes arise from having to perform a modal test on a rotating system. Conventional electromagnetic shakers are impractical and can influence the measurement being made if mounted on the hub. Further, because of the close proximity of some modal frequencies, simultaneous excitation at different points on the rotor is required.

To resolve these difficulties an investigation of a piezo-ceramic (PZT) actuation system was performed. Tests showed the suitability of the PZT material in being able to excite model scale rotor blades such that frequency response function (FRF) measurements could be made.

Initial tests compared results with conventional shakers for a non-rotating system and further measurements were performed to assess the linearity of the PZT actuation system. Final measurements acquired frequency response functions for a rotating system.

Data from the flapwise excitation tests in the range 0 to 600 rpm, with 0° collective pitch, are presented and discussed.

Model scale rotor rig

The model scale hub used for the test is based on the hub of the Westland Lynx helicopter. The 1/5 scale model with no swash plate is fully described in Ref 2. The original rotor blades designed for the model hub were not available and new composite rotor blades had to be designed and manufactured. A mould with a NACA0012 section, of chord 75 mm, was used, although, the length was slightly shorter than the original design specification. However, an exact representation of the Lynx rotor system was not required and, for the purposes of this experiment, it was sufficient only to have the dynamic characteristics of a typical rotor system. Table 1 compares the model scale rotor characteristics with those of the Lynx. A comparison of rotor tip speeds shows the rotor to be a Froude scale rotor (Ref 3)

Table 1: Comparison of Lynx and model scale characteristics

	Span m	Chord m	Rotor Speed rpm	Tip speed m/s	Required Froude scale tip speed m/s
Lynx	6.4	0.4	320	214	
Model	1.13	0.075	750	89	91

The new rotor blades were designed to suit the model rotor such that at operating speed a close match in modal frequencies was obtained with those of the Lynx helicopter. The blade construction is illustrated in figure 1. Glass fibre reinforced composite material was used to provide most of the stiffness and was wrapped as a skin layer around a foam core. The design parameters were such that around the middle chord region no glass fibre wrap was required and only a layer of film adhesive was used to protect the foam core. Mass balancing was provided by a lead leading edge weight, of suitable diameter, manufactured by extrusion.

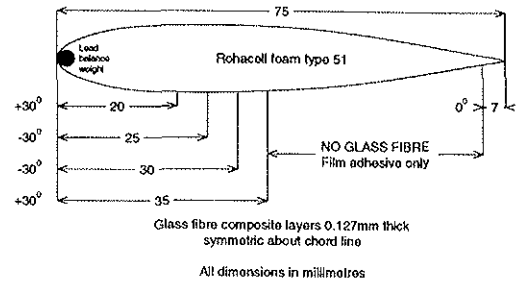

Figure 1: Model rotor blade cross-section construction details

After manufacture of the blades, the mass and structural details were measured and combined with the hub information to produce a mathematical model of the complete assembly. Natural frequency calculations were performed for both a stationary and a rotating system. The modal frequencies at operating speed were compared with those of the Lynx helicopter. A slight adjustment to the predicted modal frequencies at operating speed was made to each mode dependent upon the difference between calculated and measured frequencies for a single blade when stationary. Table 2 compares the model natural frequencies with the Lynx natural frequencies and the data is normalised with respect to rotor speed to enable a direct comparison to be made. The data shows a reasonable match for the flapwise bending modes although an exact match is not required for the purpose of this test.

Table 2: Comparison of Lynx rotor frequencies with the model scale hub

Mode type	Lynx (frequency/ rev)	Model (frequency/ rev)	% Difference
1st Lag	0.6	0.77	+28
1st Flap	1.1	1.19	+8
2nd Flap	2.8	3.01	+8
3rd Flap	4.9	4.98	+2
2nd Lag	4.5	4.99	+11
1st Torsion	6.0	6.95	+16

The rotor hub and blade assembly was mounted on a rig previously used to investigate the effectiveness of dynamic absorbers. This rig was capable of enforcing motion at the hub in 3 translations and 2 rotations or could allow the hub to be free-floating. A 6 component balance at the hub base allowed measurement of forces and moments. To obtain rotor modes it is important to allow the hub freedom to move and this freedom would be provided by the flexibility of the hub root and shaft assembly rather than the free-floating mechanism at the hub base. The free-floating mechanism is so massive in comparison to the rotor and hub that it would not provide a representative fuselage mass and for the purposes of this experiment its freedom to move was eliminated. Relying on the hub and shaft flexibility would, however, mean rotor modes would have very closely spaced natural frequencies and multi-excitation techniques would be required to resolve the separate modes. By relying on root flexibility it would be expected that the higher frequency modes would show a better separation of rotor mode frequencies. A future development of the rotor rig would involve representing fuselage mass to widen the rotor mode frequency separation. The hub assembly is shown in figure 3 and the complete rotor rig is illustrated in figure 4 .

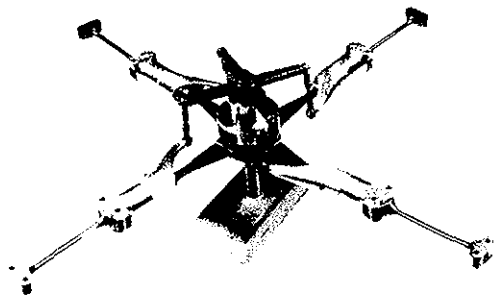

Figure 3: Scaled Lynx hub assembly

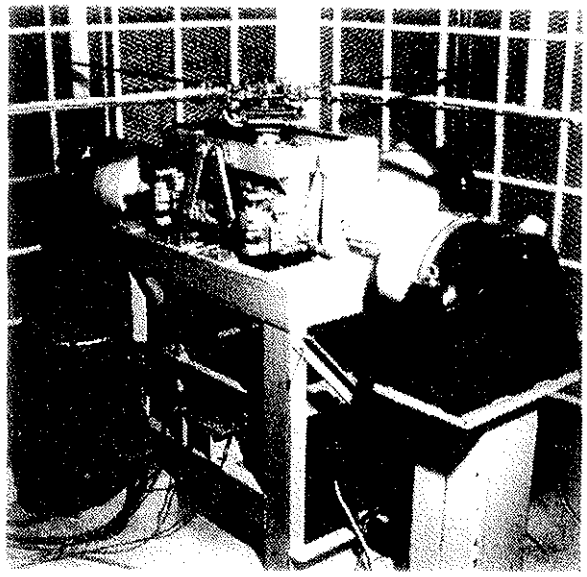

Figure 4: Rotor and hub assembly on the absorber rig

Piezo-ceramic Actuators

To determine the system modal parameters it is necessary to measure the response of the system to an excitation by a known force. Conventional techniques use accelerometers to measure the system response and force gauges combined with electromagnetic shakers to provide a known input force. Impact test methods can also be used to excite the system, however, the total amount of energy input while still remaining within a linear regime is much less than by a shaker acting over a much longer time period.

To excite a rotor while spinning involves mounting an electromagnetic shaker at the hub and forcing the blade by some mechanical arrangement. This method was successfully used to investigate a pitch-flap flutter instability of a swept tip rotor blade (Ref 4). The current test requires the measurement of rotor modes where the movement of the hub forms an important part of the system being measured. A shaker mounted on the hub would influence this result by providing extra mass and an unmeasured force input. Further, the closely spaced modal frequencies would require at least 4 shakers to be mounted at the hub which would be impractical.

To overcome these problems a different form of actuation was required which could be used on each blade. Smart material applications were considered and the feasibility of using a piezo-ceramic material, PZT (lead zirconate titanate), was assessed. PZT actuators were used on blade test samples to obtain frequency response functions (FRFs) and from these tests an understanding of the number of actuators, driving voltage and the method of attachment was obtained.

Single PZT actuators, commercially available, were of dimension 2.5" x 0.75" x 0.0075" and were supplied encapsulated in epoxy to safeguard the handling of the usually brittle material. This resulted in a thicker actuator of 0.025" and of mass 3g. The actuator shown in figure 4 is poled in the direction denoted 1 and the resulting movement in direction 3 is used to bend the rotor blade by inducing a strain along the bond interface. It is less efficient to pole in direction 1 and rely on the coupling term to provide strain in direction 3, but poling in direction 3 would require exceptionally high voltages, making for an impractical system. The physical properties of the PZT actuator are given in table 3, where the PZT strain coefficient represents the strain produced when one volt is applied for each metre of thickness.

Table 3: PZT actuator mechanical properties

Young's Modulus E33 N/m^2	Young's Modulus E11 N/m^2	Strain coefficient d33 m/V	Strain coefficient d31 m/V
$49x10^9$	$63x10^9$	$360x10^{-12}$	$250x10^{-12}$

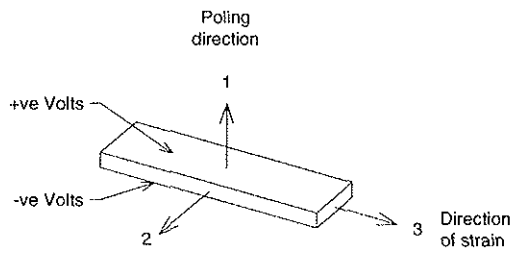

Figure 4: PZT actuator showing poling and straining directions

Typical force and extension levels obtained from these actuators would be in the order of 30 N when fully constrained or just over 7 μm when unconstrained. The maximum force of 30 N is only developed when the actuator is totally restrained and any application allowing movement, such as the bending of a beam, would result in less force being developed. A force equilibrium is set up across the bond interface, where the PZT extension balances that of the structure being excited. For a typical test rotor blade of 0.5m length with two PZT actuators attached at the root, a tip deflection of 0.4 mm would be expected for 100V static excitation. Applying a voltage at increasing frequency would produce large displacements at rotor blade resonance when it is only necessary for the PZT actuators to overcome the system damping.

To drive the PZT actuators and obtain a reasonable force output a high voltage signal of 100V pk is required. A suitable amplifier was designed and built using components specifically manufactured for PZT elements. A high voltage power supply with sufficient current capability was necessary to operate the amplifier. Adding PZT actuators to increase the force input was offset by the need for high current levels from the amplifier. Similarly, the requirement for a frequency response up to 100 Hz also made demands on the amplifier due to the capacitance of the PZT units. The final actuator was formed from 4 separate PZT units wired in parallel and bonded to the upper and lower surface of the rotor blade (figure 5). To induce bending in the rotor blade, the voltage supplied to the two upper units was in anti-phase to that supplied to the lower units.

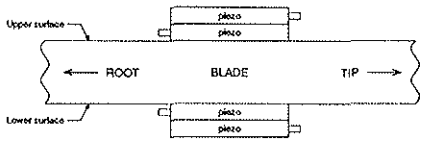

Figure 5 PZT attachment to rotor blades

Unlike a conventional electromagnetic shaker attachment the point of excitation used for PZT is permanent due to the bonding of the device to the rotor blade surface. It is, therefore, important to determine the optimum location of the PZT actuator to excite the desired modes. This first test series was aimed at measuring flapwise bending modes and a sensible location for the actuator would have been at the hub root. This would have enabled an excitation of all flapwise bending modes, however, space limitations prevented this location being chosen and so an alternative site on the rotor blade was used. To excite any mode it is desirable to position the device at a point of greatest curvature for the mode shape in question. Points of greatest curvature were calculated for a 2nd and 3rd flapwise bending mode and a compromise location to suit both modes was chosen. No attempt was made to excite the fundamental flapwise bending mode because the stiff root condition was unlikely to yield easily measurable rotor modes and the aerodynamic damping, when rotating, would also make the measurement difficult.

To excite torsion modes the PZT actuators were bonded to the blade at an angle of 45° with respect to the blade chord. The actuators were not used in this test series, but are intended for further work.

Rotor blade instrumentation

Accelerometers provide a convenient way of measuring the mode shapes of a system. The resulting shapes, based on accelerations, which can be easily converted to velocity or displacement, are the usual theoretically derived variables. Unfortunately, the rotating system, imparts a large acceleration on the response transducers, clouding the acceleration from the vibrating modes and thus leading to incorrect mode shapes. An account of the distortion due to rotation is presented in (Ref 5).

A solution to the difficulty of measuring mode shapes using accelerometers is to use alternative transducers, which are not affected by the rotation. Strain gauges were used in this case, configured in balanced bridges and calibrated to measure bending and torsion moments. However, there is no direct transformation from bending and torsion moments to accelerations without referring to a structural model. Any theoretical validation of mode shapes, therefore, would have to be done by comparing bending and torsion moments.

Two sets of non-rotating measurements were made one using accelerometers and another using strain gauges. Each of these tests were performed twice, once with conventional shaker excitation and once with PZT excitation. The main objective of this duplication was to compare results from the new PZT excitation technique with the results from a conventional test configuration. The photograph of figure 6 shows the rotor undergoing a non-rotating shake test. The electromagnetic shakers are suspended from a roof fixing and attached to the hub near the rotor blade root. The flapwise PZT actuator is bonded close to the rotor blade mid-position and the torsion PZT actuator is located near to the rotor blade root. Accelerometer positions are along the rotor blade length and attached using low mass foam mounting blocks to provide orthogonal measurement directions. Strain gauge positions are also visible along the blade length.

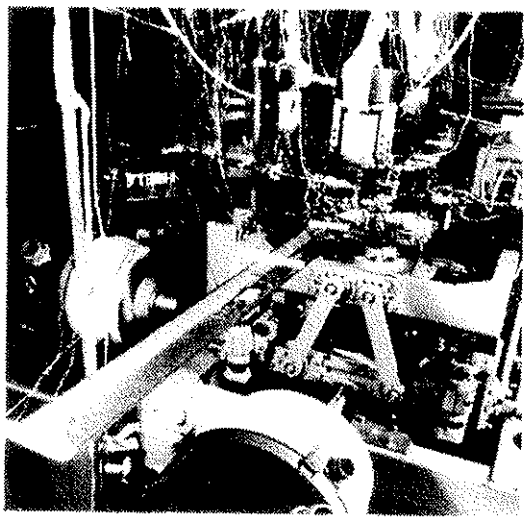

Figure 6: Rotor system undergoing non-rotating shake test.

The accelerometer and strain gauge layouts, which are the same for each rotor blade and hub arm, are illustrated below in figure 7

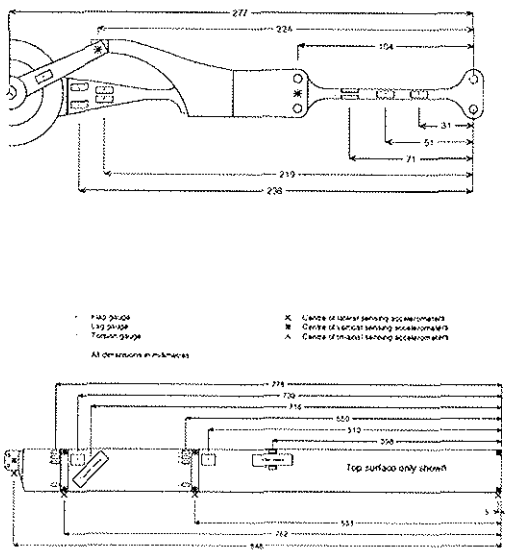

Figure 7: Rotor blade and hub strain gauge / accelerometer arrangement.

A total of 56 accelerometers and 52 strain gauges were used to measure response data. The accelerometers were calibrated dynamically prior to use, with respect to a force gauge, using a known mass (Ref 6). The strain gauges were calibrated with the hub fully assembled.

Signal conditioning was provided by a bank of onboard amplifiers figure 8, designed and manufactured in-house and installed below the hub. The signals were passed to

the data acquisition hardware via an 80-way slip ring assembly at the bottom of the main drive shaft.

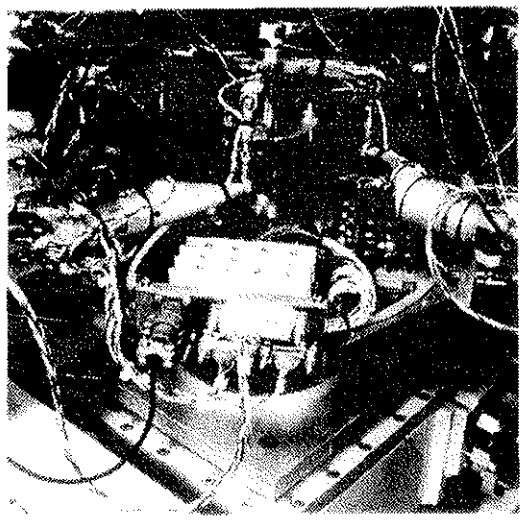

Figure 8: Signal conditioning amplifiers

Data acquisition and analysis

Response and force data was collected via a SCADAS 2 data acquisition system controlled by an HP 715 9000 series workstation running LMS CADA-X software. The FRF data was stored on disc prior to modal analysis using the same LMS CADA-X software.

A multiple-input multiple-output (MIMO) test technique was used to provide an even distribution of excitation energy throughout the structure, and also to help in identifying closely spaced natural frequencies. Band-limited uncorrelated noise was input as the excitation signal to each actuator, with the band determined by the frequency range of interest for the test. Post measurement analysis of the measured cross-spectrum matrix within the testing software gave the required FRFs.

Preliminary test measurements indicated noisy and ill-defined FRFs with increasing rotor speed. Low pass digital filters in the SCADAS were unsuitable for solving this problem since the analogue to digital conversion of the signal had to be performed prior to filtering, resulting in a low signal to noise ratio due to poor bit resolution. This was solved by placing matched filters in the data lines before data acquisition with a filter setting of 124 Hz low pass. Only 20 of these filters were available at the time of testing so a reduced data set of 4 transducers for each blade had to be defined. This set included all of the flapwise bending strain gauge stations on the blade and a further flapwise bending station at the hub root.

Modal analysis was provided by the Frequency Domain Direct Parameter Identification technique resident within the LMS CADA-X software. Natural frequencies, damping values and mode shapes can be estimated for several references and modes simultaneously (Ref 7).

FRF Comparison between PZT and electro-magnetic excitation

Reciprocity plots are shown for both the non-rotating shaker tests and the PZT excitation tests (figure 9 to figure 12). The reciprocity for the 3rd flapwise bending mode is reasonable for all the configurations presented, even for the reciprocity between blades 1 and 2. The reciprocity data all involve the transfer of force across the hub and because of the lack of flexibility in the root condition of the hub, especially for the lower order modes, a poor result could be expected. However, in general, around the resonance conditions the data appears to be good, apart from the conventional shaker data, where some mismatch is apparent for the second flapwise bending.

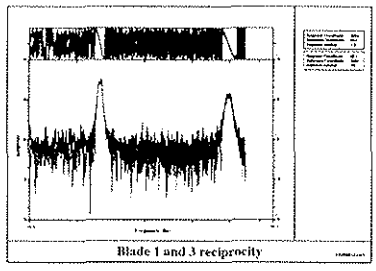

Figure 9: Reciprocity , PZT excitation from blade 1 to 3

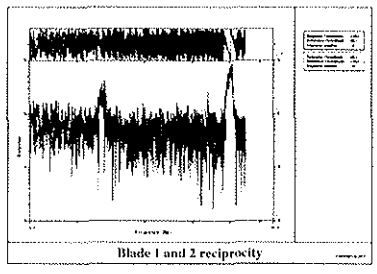

Figure 10: Reciprocity, PZT excitation from blade 1 to 2

Examination of the shaker derived data for the second flap mode shapes (appendix A) reveals four independent modes shapes with no coupling across the shaft boundary. Comparison with the same modes excited by PZT actuators (appendix A) reveals a coupling between opposite blades forming symmetric and anti-symmetric mode shapes. The modal frequencies derived from the shaker measurements are also slightly higher (about 5%) than those derived from the PZT measurements. It is probable that the higher frequencies and uncoupled mode shapes are caused by extra rotational stiffness being imparted from the shaker attachment push-rods. These push-rods should be stiff enough to provide a means of applying load to the structure without buckling, but be flexible enough to reduce the effects of adding stiffness to the structure. For the second flapwise bending mode in question it would appear that more flexibility in the shaker push-rods is needed. This demonstrates the benefits of PZT actuators for this type of application.

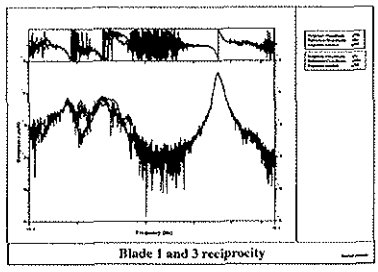

Figure 11: Reciprocity, shaker excitation from blade 1 to 3

Examination of the third flapwise bending mode shapes (appendix A) shows a much better agreement between those derived by shaker and PZT actuator. The shaker data is still slightly higher in modal frequency prediction (0.4 to 1.6 %), which is probably still due to the push rod stiffness having some effect.

It is clear in the data presented at appendix A that there are problems with one of the accelerometers on the tip of rotor blade 4. There is also a phase difference in mode shapes when comparing data derived from shakers and the PZT actuators. This is because the voltage used to drive the PZT actuator is being used as the 'force' part of the measurement. Calibrations have yet to be applied to the PZT voltage 'force' data and so direct comparisons of magnitude with the shaker derived mode shapes are not of value.

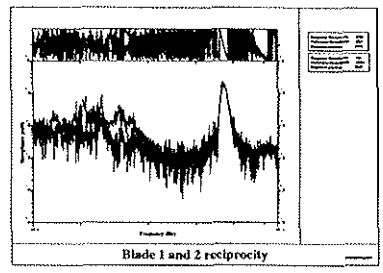

Figure 12: Reciprocity, shaker excitation from blade 1 to 2

Strain gauge and PZT frequency response functions

Mode shapes derived from bending moment measurements made while the system was rotating are presented at appendix B. All the measurements were made with 0 degrees collective pitch up to a maximum rotor speed of 600 rpm. The mode shapes are complex making it very difficult to visualise the nature of the mode by plotting the displaced shape. To help in comparing the mode shapes at the various rotor speeds real and imaginary components of the displacements are displayed for each blade.

At 0 rpm the second flap mode shapes only show coupling across opposite rotor blades. Each of the four mode shapes has the same maximum bending moment at the blade root and damping levels in the modes are similar at approximately 0.5 % of critical. The patterns formed by the blades represent symmetric and anti-symmetric shapes, with the blade combination 2 and 4 having a slightly lower frequency than the blade combination 1 and 3.

When rotating, the mode shapes gradually become more complex and this is more apparent with the cyclic modes of the 2nd flapwise bending. Here the previously dormant blades respond but with a 90° phase shift.

At 400 rpm a well defined set of shapes appear. Modes 2 and 3 are collective and non-reactive respectively while the remaining two modes are cyclic.

Increasing rotor speed further to 600 rpm results in a collective mode with a much increased relative natural frequency and is now mode 4. The non-reactive mode is still close to the cyclic modes and is mode 3.

The sequence of modes for the third order flapwise bending mode shapes at 0 rpm indicate a greater coupling between all rotor blades than was seen for the

second bending mode shape. The first two shapes at 0 rpm are orthogonal anti-symmetric mode shapes, the third is a collective mode shape and the final mode in the set is non-reactive.

Increasing rotor speed through to 600 rpm reveals similar patterns in mode shapes to those seen for the second flapwise bending.

Data has been compared with that obtained using electro-magnetic shakers and in some applications has been shown to be a superior excitation technique.

Frequency response data has been measured for rotating and non-rotating systems using PZT actuation and a subsequent analysis has derived rotor mode shapes for the different rotor speed conditions.

Further work

The results presented demonstrate the success in using a PZT actuated system in measuring modal characteristics of a rotating system. To complete the exercise, further test cases are required with PZT excitation of the torsion modes of the rotor and similarly for the rotor lag modes, although the drive system using PZT actuators for lagwise excitation has not yet been tested.

Improvements in the measurement technique may be made by sampling data on a rotor azimuth clock rather than a real time clock. Current measurement times span many rotations and variations in rotor speed mean data is not taken at the same azimuth point. Improvements may be obtained, particularly with averaging, if data were collected at the same azimuth points for all the rotations.

The current experiment relies on the hub flexibility to be able to observe rotor modes. To validate theoretical analyses using this data would depend on having a good representation of the hub root condition. This may present some difficulties and it would be better to provide a root condition allowing vertical movement and possibly rotations at the root which did not rely on the hub flexibility. This would be easier to model and would also provide a better split in modal frequencies making it simpler to measure and analyse.

Conclusions

PZT actuation has been demonstrated as a feasible method for exciting structures to enable the measurement of frequency response functions for the determination of modal parameters.

References

1 Hansford R. E., *'Considerations in the development of the Coupled Rotor Fuselage Model'*, AHS 48th Annual National Forum, Washington D C, June 1992.

2 Cansdale R, *'An aeroelastic model helicopter rotor'*, CP No 1288, Structures Dept., RAE Farnborough, 1974.

3 Hatch C, *'The dynamic scaling and development of model helicopter rotor blades for the RAE 24ft wind tunnel test rig'*, TR85052, Materials and Structures Dept., RAE Farnborough, May 1985

4 Walker W. R., Hatch C, *'Pitch-flap flutter instability of a swept-tip model rotor blade'*, Paper 6.12, 13th European Rotorcraft Forum, September 1987.

5 Gaukroger D. R., *'A note on the use of accelerometers to measure mode shapes of a rotating helicopter blade'*, Tech. Memo. Structure 928, RAE Farnborough, August 1978.

6 Ewins D. J., *'Modal testing : Theory and Practice'*, Research Studies Press Ltd., Letchworth, Hertfordshire, England. John Wiley & Sons Inc. 1984

7 LMS International, *'LMS CADA-X Modal analysis manual'*, P/N X.P50.1 Revision 3.3, LMS International, 1994

Appendix A

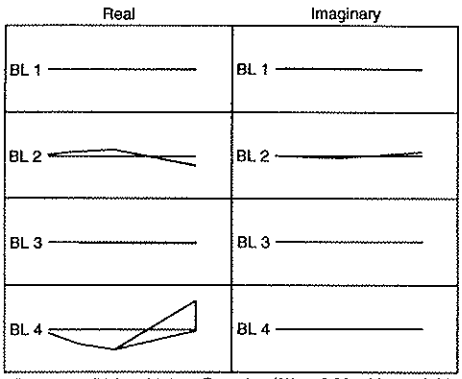

Frequency (Hz) = 22.26 Damping (%) = 0.96 Max = 3.01
Shaker derived 2nd Flap Mode 1

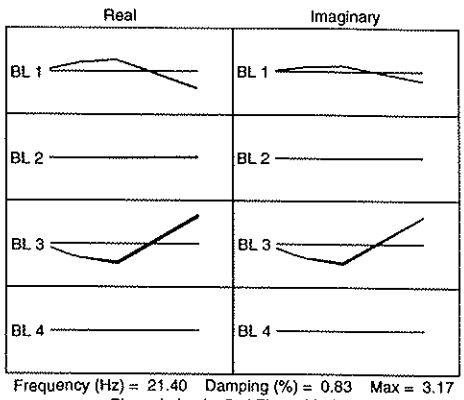

Frequency (Hz) = 21.40 Damping (%) = 0.83 Max = 3.17
Piezo derived 2nd Flap Mode 1

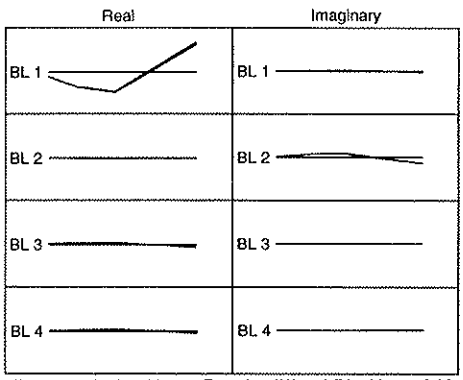

Frequency (Hz) = 22.67 Damping (%) = 1.74 Max = 2.68
Shaker derived 2nd Flap Mode 2

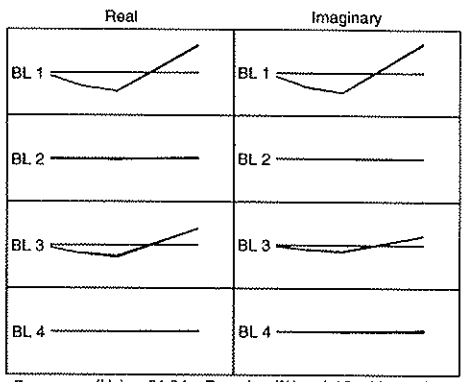

Frequency (Hz) = 21.84 Damping (%) = 1.18 Max = 3.17
Piezo derived 2nd Flap Mode 2

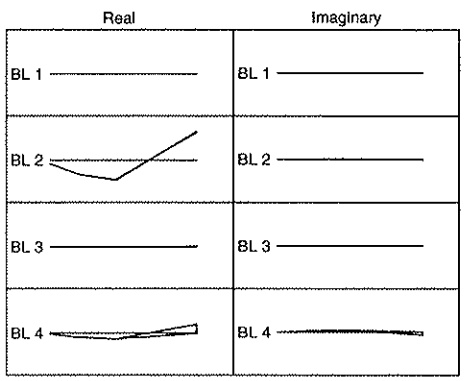

Frequency (Hz) = 22.76 Damping (%) = 1.52 Max = 3.27
Shaker derived 2nd Flap Mode 3

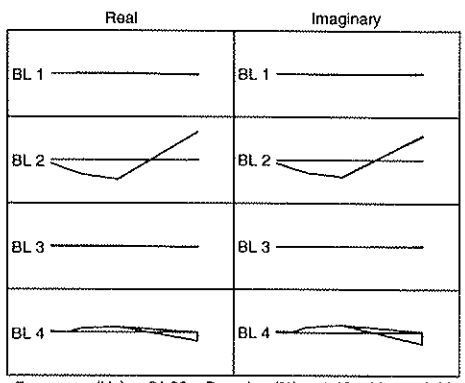

Frequency (Hz) = 21.93 Damping (%) = 1.43 Max = 3.30
Piezo derived 2nd Flap Mode 3

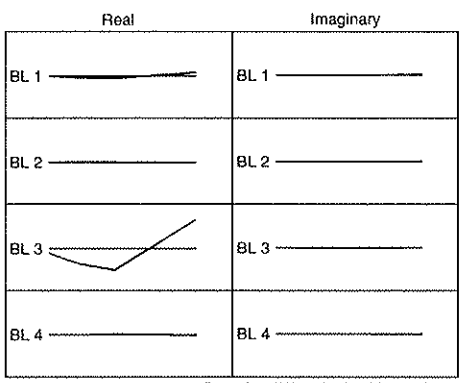

Frequency (Hz) = 23.92 Damping (%) = 0.78 Max = 2.71
Shaker derived 2nd Flap Mode 4

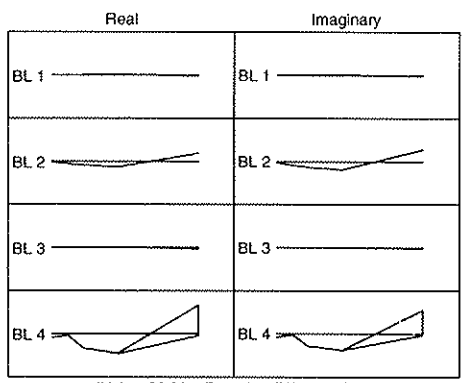

Frequency (Hz) = 22.38 Damping (%) = 1.10 Max = 3.59
Piezo derived 2nd Flap Mode 4

Appendix A

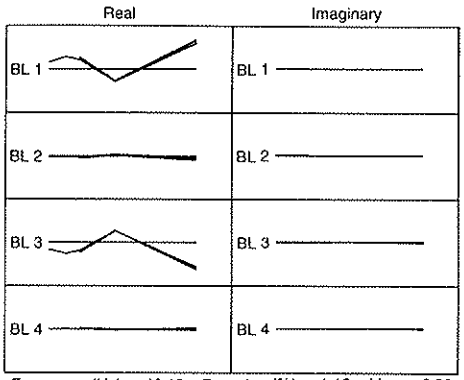

Frequency (Hz) = 46.13 Damping (%) = 1.19 Max = 2.39
Shaker derived 3rd Flap Mode 1

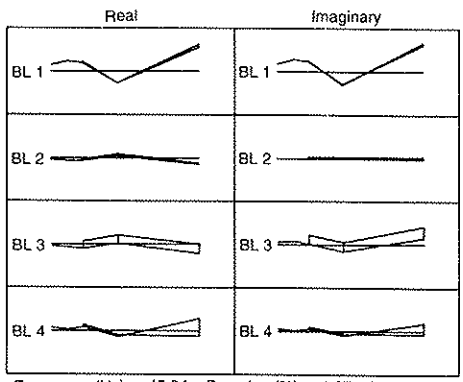

Frequency (Hz) = 45.94 Damping (%) = 1.67 Max = 9.02
Piezo derived 3rd Flap Mode 1

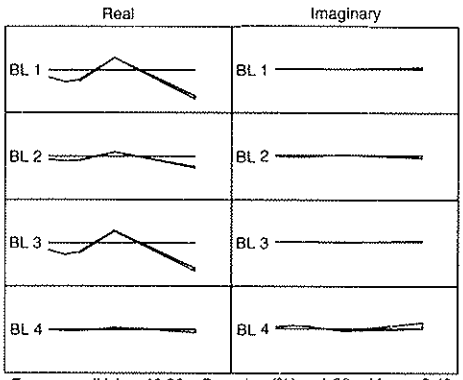

Frequency (Hz) = 46.93 Damping (%) = 1.39 Max = 2.40
Shaker derived 3rd Flap Mode 2

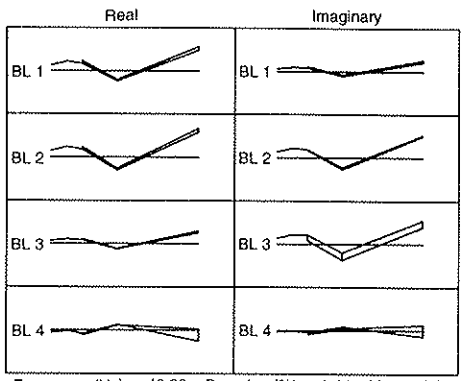

Frequency (Hz) = 46.28 Damping (%) = 1.44 Max = 6.99
Piezo derived 3rd Flap Mode 2

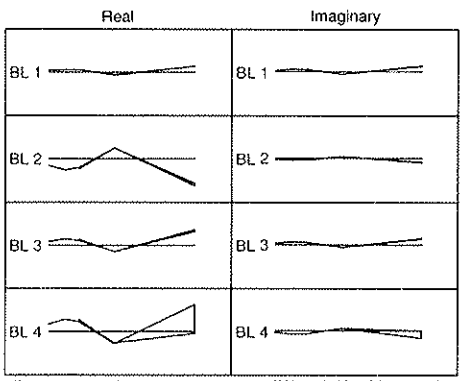

Frequency (Hz) = 47.17 Damping (%) = 1.43 Max = 2.24
Shaker derived 3rd Flap Mode 3

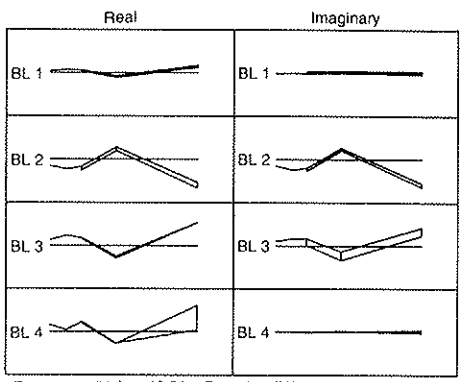

Frequency (Hz) = 46.51 Damping (%) = 1.52 Max = 9.17
Piezo derived 3rd Flap Mode 3

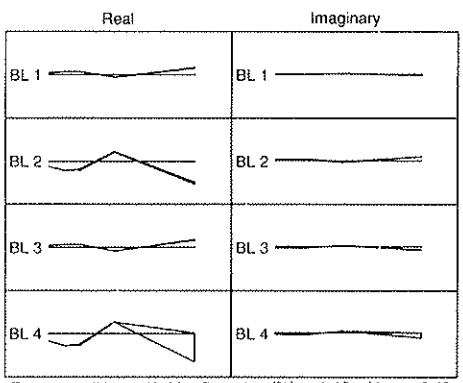

Frequency (Hz) = 47.90 Damping (%) = 1.48 Max = 2.49
Shaker derived 3rd Flap Mode 4

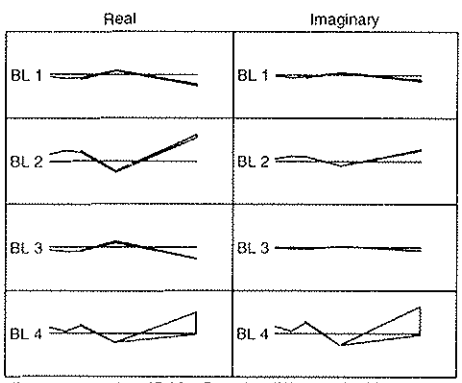

Frequency (Hz) = 47.12 Damping (%) = 1.74 Max = 9.23
Piezo derived 3rd Flap Mode 4

Appendix B

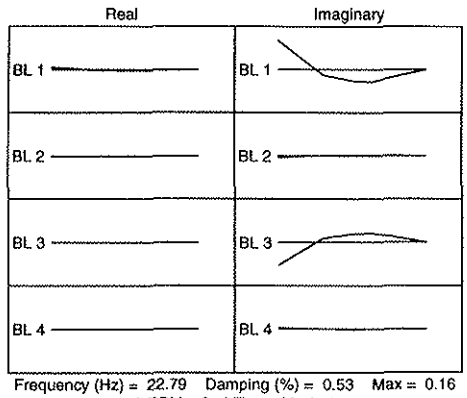

Frequency (Hz) = 22.79 Damping (%) = 0.53 Max = 0.16
0 RPM 2nd Flap Mode 1

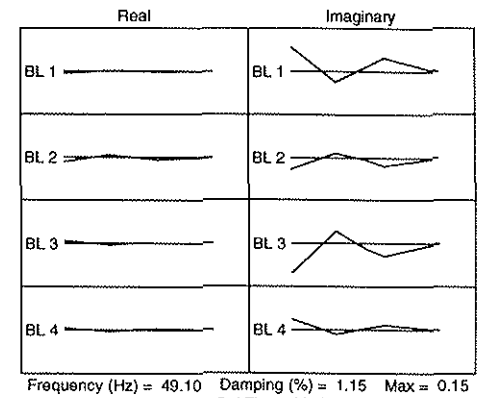

Frequency (Hz) = 49.10 Damping (%) = 1.15 Max = 0.15
0 RPM 3rd Flap Mode 1

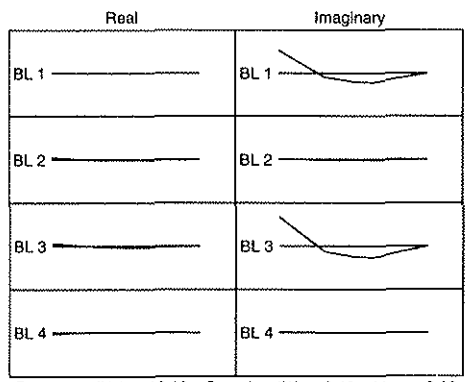

Frequency (Hz) = 23.18 Damping (%) = 0.46 Max = 0.18
0 RPM 2nd Flap Mode 2

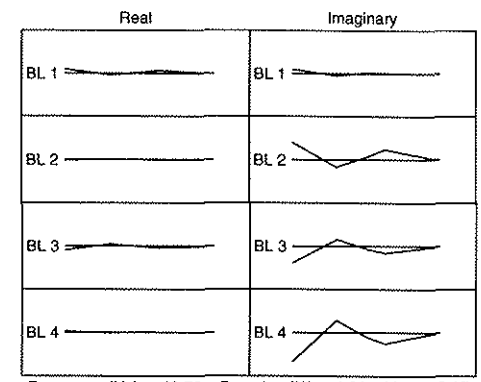

Frequency (Hz) = 49.72 Damping (%) = 1.31 Max = 0.17
0 RPM 3rd Flap Mode 2

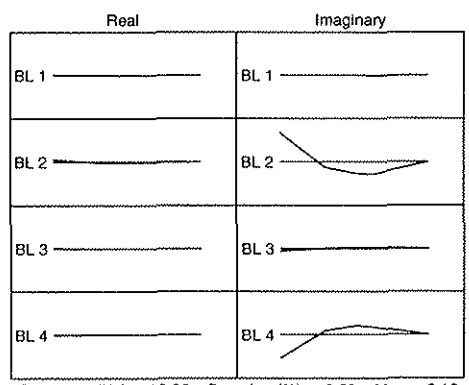

Frequency (Hz) = 23.25 Damping (%) = 0.53 Max = 0.16
0 RPM 2nd Flap Mode 3

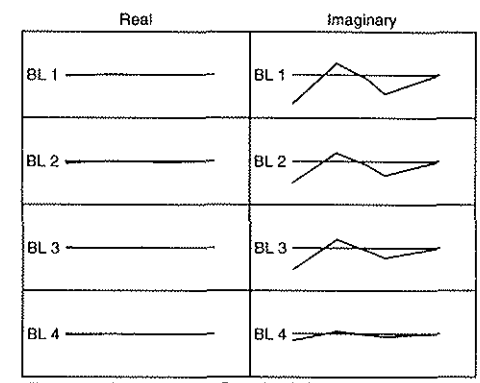

Frequency (Hz) = 50.03 Damping (%) = 1.26 Max = 0.11
0 RPM 3rd Flap Mode 3

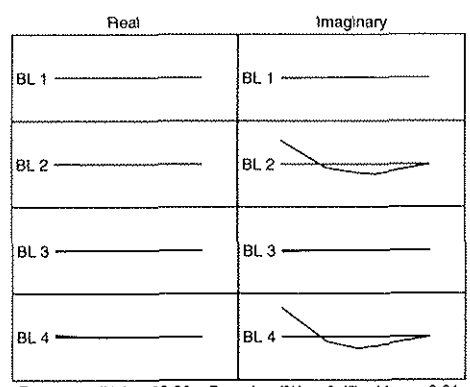

Frequency (Hz) = 23.60 Damping (%) = 0.47 Max = 0.21
0 RPM 2nd Flap Mode 4

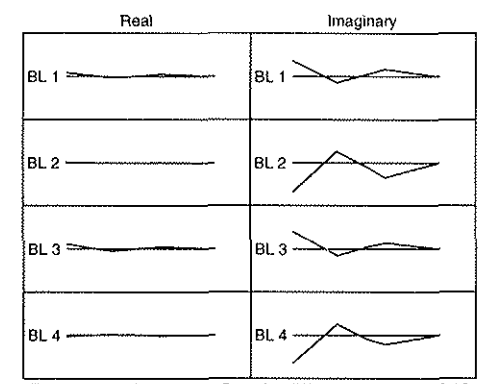

Frequency (Hz) = 50.63 Damping (%) = 0.73 Max = 0.12
0 RPM 3rd Flap Mode 4

Appendix B

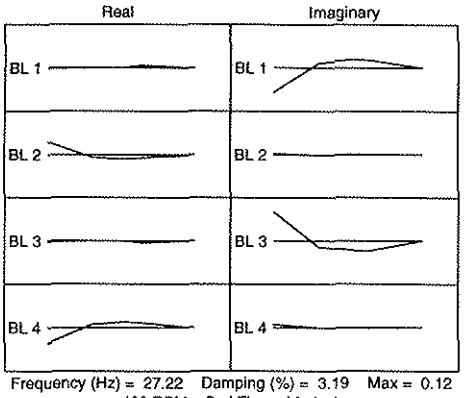

Frequency (Hz) = 27.22 Damping (%) = 3.19 Max = 0.12
400 RPM 2nd Flap Mode 1

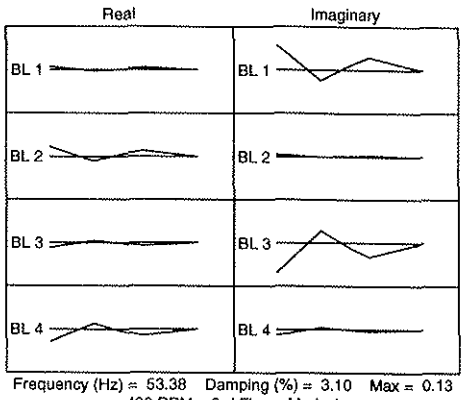

Frequency (Hz) = 53.38 Damping (%) = 3.10 Max = 0.13
400 RPM 3rd Flap Mode 1

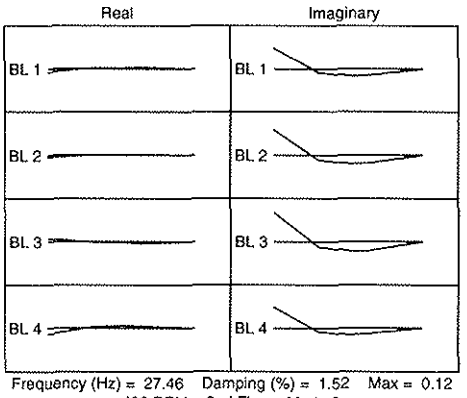

Frequency (Hz) = 27.46 Damping (%) = 1.52 Max = 0.12
400 RPM 2nd Flap Mode 2

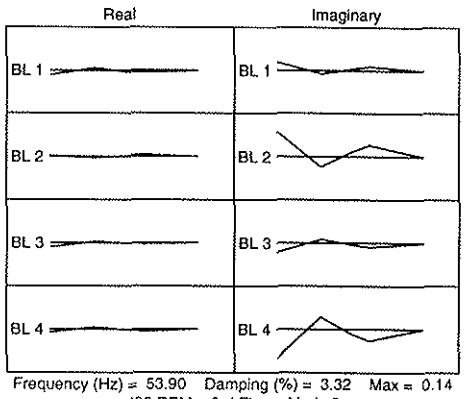

Frequency (Hz) = 53.90 Damping (%) = 3.32 Max = 0.14
400 RPM 3rd Flap Mode 2

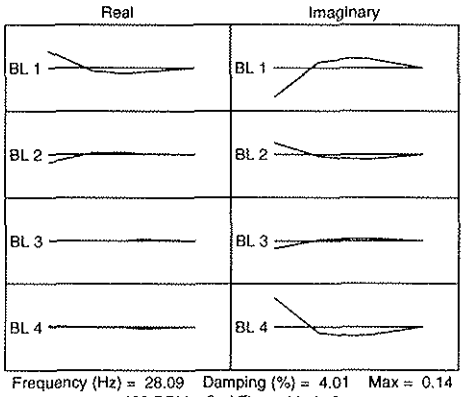

Frequency (Hz) = 28.09 Damping (%) = 4.01 Max = 0.14
400 RPM 2nd Flap Mode 3

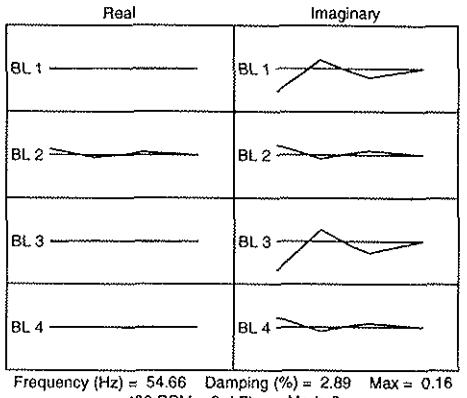

Frequency (Hz) = 54.66 Damping (%) = 2.89 Max = 0.16
400 RPM 3rd Flap Mode 3

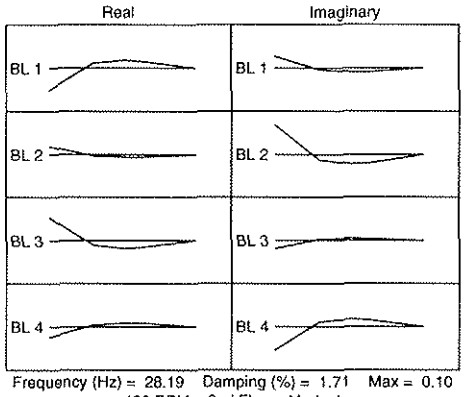

Frequency (Hz) = 28.19 Damping (%) = 1.71 Max = 0.10
400 RPM 2nd Flap Mode 4

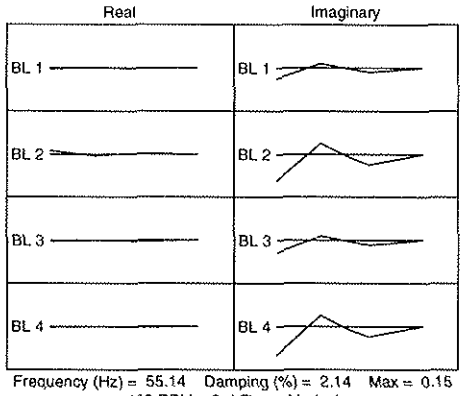

Frequency (Hz) = 55.14 Damping (%) = 2.14 Max = 0.15
400 RPM 3rd Flap Mode 4

Appendix B

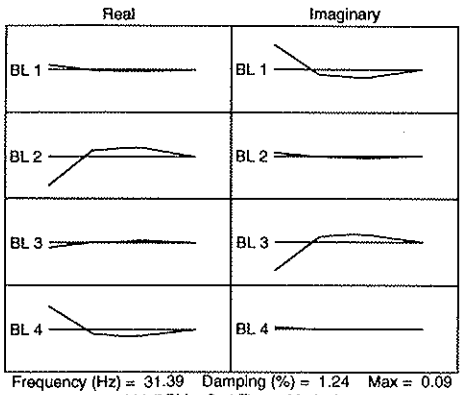

Frequency (Hz) = 31.39 Damping (%) = 1.24 Max = 0.09
600 RPM 2nd Flap Mode 1

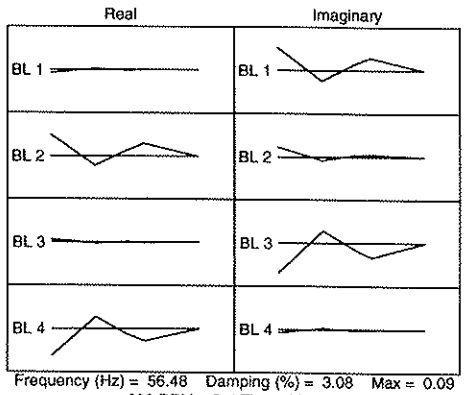

Frequency (Hz) = 56.48 Damping (%) = 3.08 Max = 0.09
600 RPM 3rd Flap Mode 1

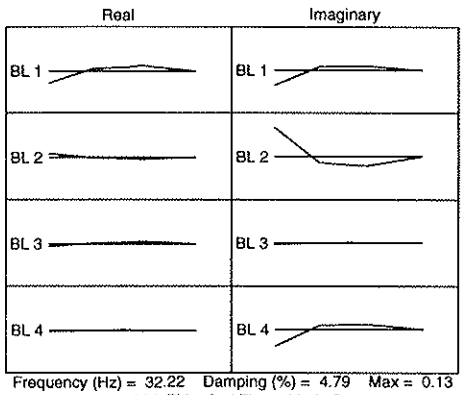

Frequency (Hz) = 32.22 Damping (%) = 4.79 Max = 0.13
600 RPM 2nd Flap Mode 2

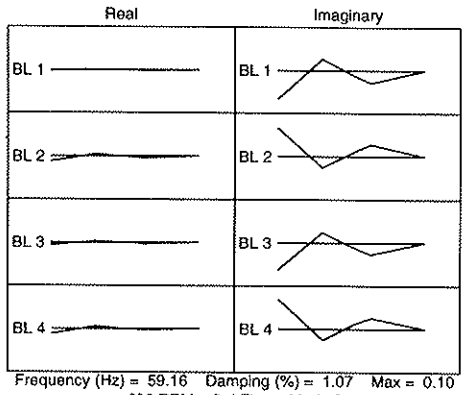

Frequency (Hz) = 59.16 Damping (%) = 1.07 Max = 0.10
600 RPM 3rd Flap Mode 2

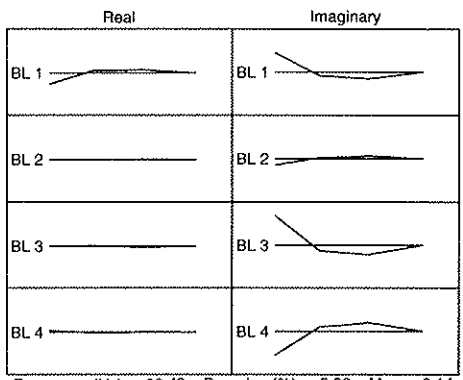

Frequency (Hz) = 32.43 Damping (%) = 5.98 Max = 0.14
600 RPM 2nd Flap Mode 3

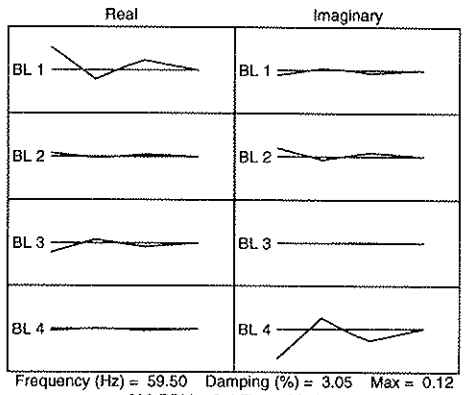

Frequency (Hz) = 59.50 Damping (%) = 3.05 Max = 0.12
600 RPM 3rd Flap Mode 3

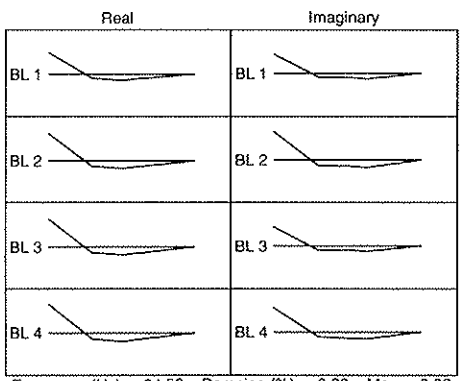

Frequency (Hz) = 34.56 Damping (%) = 0.23 Max = 0.02
600 RPM 2nd Flap Mode 4

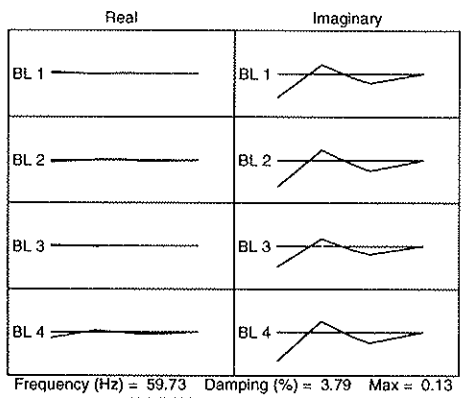

Frequency (Hz) = 59.73 Damping (%) = 3.79 Max = 0.13
600 RPM 3rd Flap Mode 4